J Mol Model (2013) 19:1819–1834
DOI 10.1007/s00894-012-1745-0

ORIGINAL PAPER

Quantum chemical study of silanediols as metal binding groups for metalloprotease inhibitors

Igor S. Ignatyev · Manuel Montejo · Pilar Gema Rodríguez Ortega · Juan Jesús López González

Received: 16 October 2012 / Accepted: 18 December 2012 / Published online: 15 January 2013

Abstract DFT (B3LYP and M06L) as well as *ab initio* (MP2) methods with Dunning cc-pVnZ (n=2,3) basis sets are employed for the study of the binding ability of the new class of protease inhibitors, i.e., silanediols, in comparison to the well-known and well-studied class of inhibitors with hydroxamic functionality (HAM). Active sites of metalloproteases are modeled by $[R_3M\text{-}OH_2]^{2+}$ complexes, where R stands for ammonia or imidazole molecules and M is a divalent cation, namely zinc, iron or nickel (in their different spin states). The inhibiting activity is estimated by calculating Gibbs free energies of the water displacement by metal binding groups (MBGs) according to: $[R_3M\text{-}OH_2]^{2+}$ + MBG → $[R_3M\text{-}MBG]^{2+}$ + H_2O. The binding energy of silanediol is only a few kcal mol^{-1} inferior to that of HAM for zinc and iron complexes and is even slightly higher for the triplet state of the $(NH_3)_3Ni^{2+}$ complex. For both MBGs studied in the ammonia model the binding ability is nearly the same, i.e., $Fe^{2+}(t) > Ni^{2+}(t) > Fe^{2+}(q) > Ni^{2+}(s) > Zn^{2+}$. However, for the imidazole model the order is slightly different, i.e., $Ni^{2+}(t) > Fe^{2+}(t) > Fe^{2+}(q) > Ni^{2+}(s) \geq Zn^{2+}$. Equilibrium structures of the R_3Zn^{2+} complexes with both HAM and silanediol are characterized by the monodentate binding, but the bidentate character of binding increases on going to iron and nickel complexes. Two types of intermediates of the water displacement reactions for $[(NH_3)_3M\text{-}OH_2]^{2+}$ complexes were found which differ by the direction of the attack of the MBG. Hexacoordinated complexes exhibit bidentate bonding of MBGs and are lower in energy for M=Ni and Fe. For Zn penta- and hexacoordinated complexes have nearly the same energy. Intermediate complexes with imidazole ligands have only octahedral structures with bidentate bonding of both HAM and dimethylsilanediol molecules.

Keywords *ab initio* · Binding energy · DFT · Metal binding groups · Metalloproteases inhibitors · Silanediol functionality

M. Montejo · P. G. Rodríguez Ortega · J. J. L. González (✉)
Department of Physical and Analytical Chemistry. Experimental Sciences Faculty, University of Jaén, Campus "Las Lagunillas", 23071 Jaen, Spain
e-mail: jjlopez@ujaen.es

I. S. Ignatyev
Department of Chemistry, Radiochemistry Laboratory, St. Petersburg State University, St. Petersburg 199034, Russia

Introduction

Metalloproteases are enzymes which play a crucial role in the catalysis of a vast number of physiological processes including numerous human diseases such as cancer and hypertension. The effective inhibiting of these processes is one of the main goals in drug design. The active catalytic site of metalloproteases is a M^{2+} cation incorporated in enzymes [1–4]. The metal ion as a catalytic enzyme site is tetrahedrally coordinated by three amino acids (most frequently by histidine) and an exchangeable water molecule [1–10]. The mechanism of the catalytic activity of proteases still remains controversial [3, 11–14] but one of the plausible ways of metal site catalytic activity is the interaction with substrate which may proceed when the coordinated water molecule is displaced to allow the access of the substrate to the metal center [15]. Replacement of this water molecule by the metal binding group (MBG) inhibits the catalytic activity of the enzyme.

Thus, the ability of a MBG to displace a water molecule characterizes the inhibiting properties of this group. Computational models for the estimation of the strength of interaction between the binding group and a metal cation incorporated into enzymes may be very useful for the design

of drugs acting as inhibitors of enzymes. Due to the crucial role of zinc in the activity of enzymes [3], the majority of studies have been focused on the search of the potent zinc binding groups (ZBG). However, many potent inhibitors failed clinically because they bind stronger to metals other than zinc [16] therefore the selectivity of the binding group toward zinc is a desirable property of the drug candidate.

One the most important examples from the standpoint of clinical use has been the inhibition of angiotensin-converting enzyme (ACE). Inhibition of this enzyme is a classic medicinal chemistry approach to the treatment of hypertension [17, 18]. Numerous molecules, most of which contain metal chelators with carboxylic, amide or hydroxamate functionalities were used as ACE inhibitors [19–21]. During the last 15 years, new effective inhibitors with geminal silanediol functionality were proposed by the group of Prof. Sieburth [22–26].

There are several works in which the interaction of chelators with metal ions of enzymes are studied by quantum chemical methods [27–46]. Since the theoretical treatment of real

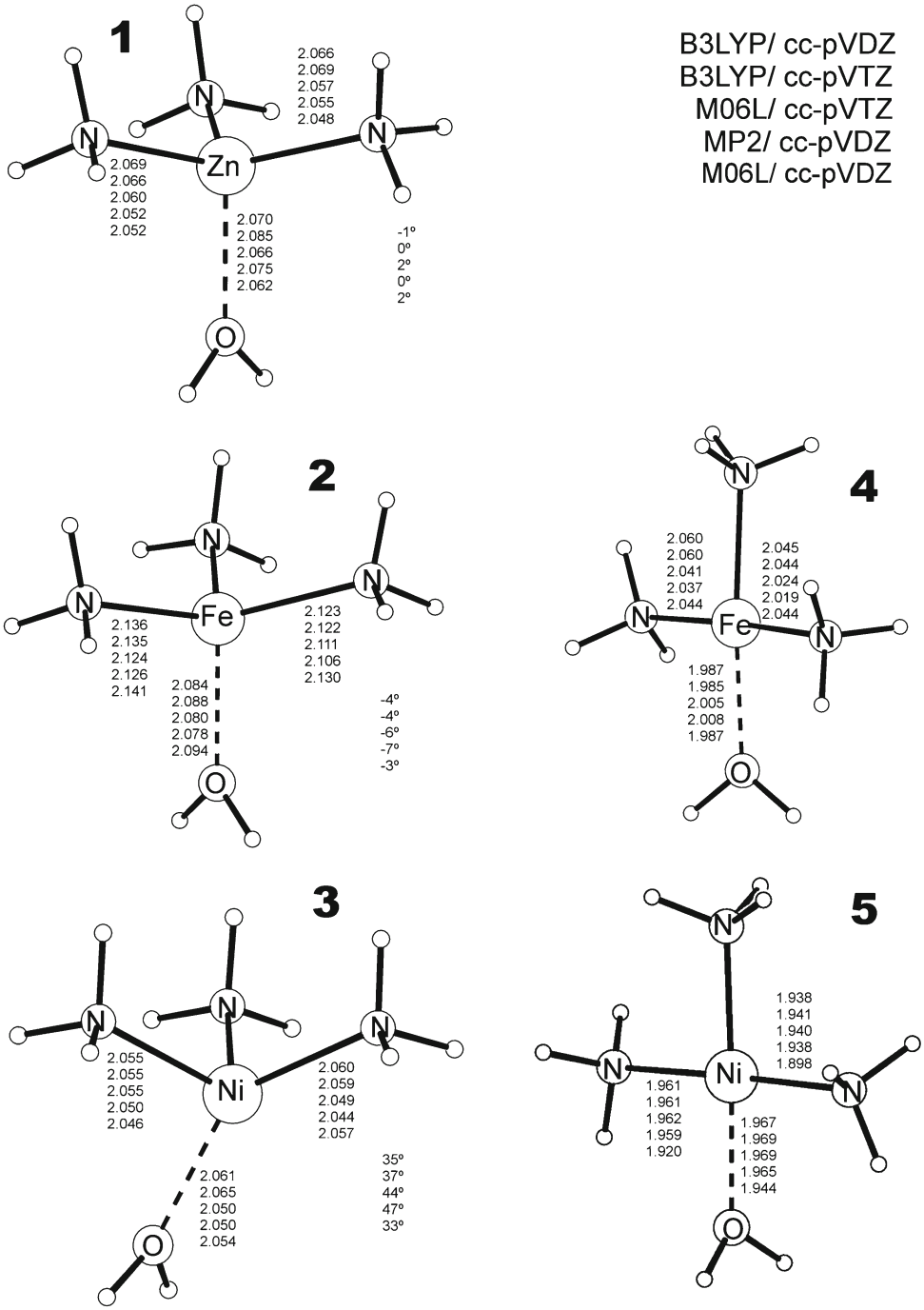

Fig. 1 Equilibrium structures (bond lengths in Å) of metalloprotease active site models with ammonia ligands

enzyme structures is out of the reach for the state-of-the-art computational DFT and *ab initio* methods, in the computational models amino acid residues in enzymes are mimicked using nitrogen containing molecules such as ammonia or imidazole rings. Most of these studies deal with molecules with hydroxamate functionality as most widely used and potent metal binding group [43–45]. However, Šramko, Garaj, and Remko [35] used the ONIOM approach (combined B3LYP-MNDO methods) for the study of the interaction between 29 neutral and deprotonated enzyme inhibitors (including silanediol) and zinc cation with three first-shell ligands as models of active site of angiotensin-converting enzyme.

Dobbs et al. [36] predicted structures of complexes between the model of peptide deformylase, consisting of a metal dication (iron-(II), cobalt (II), nickel(II), or zinc (II)) wrapped in a tridentate spectator ligand 2-methyl-1-([methyl-(2-pyridin-2-ylethyl)-amino] propane-2-thiolate (PATH), and various metal binding groups. The study was carried out using theoretical methods of higher level (B3LYP/DGDZVP single-point energies on BP86/DGDZVP optimized structures) and for iron, nickel and cobalt the structure of complexes in different spin states was revealed. However, silanediols were not included in the list of inhibitors.

Here we present the results of the optimization at the DFT levels (B3LYP and M06L) of complexes between the enzyme models (tridentate amino acid residues with an exchangeable water molecule) and dimethylsilanediol (as a relatively

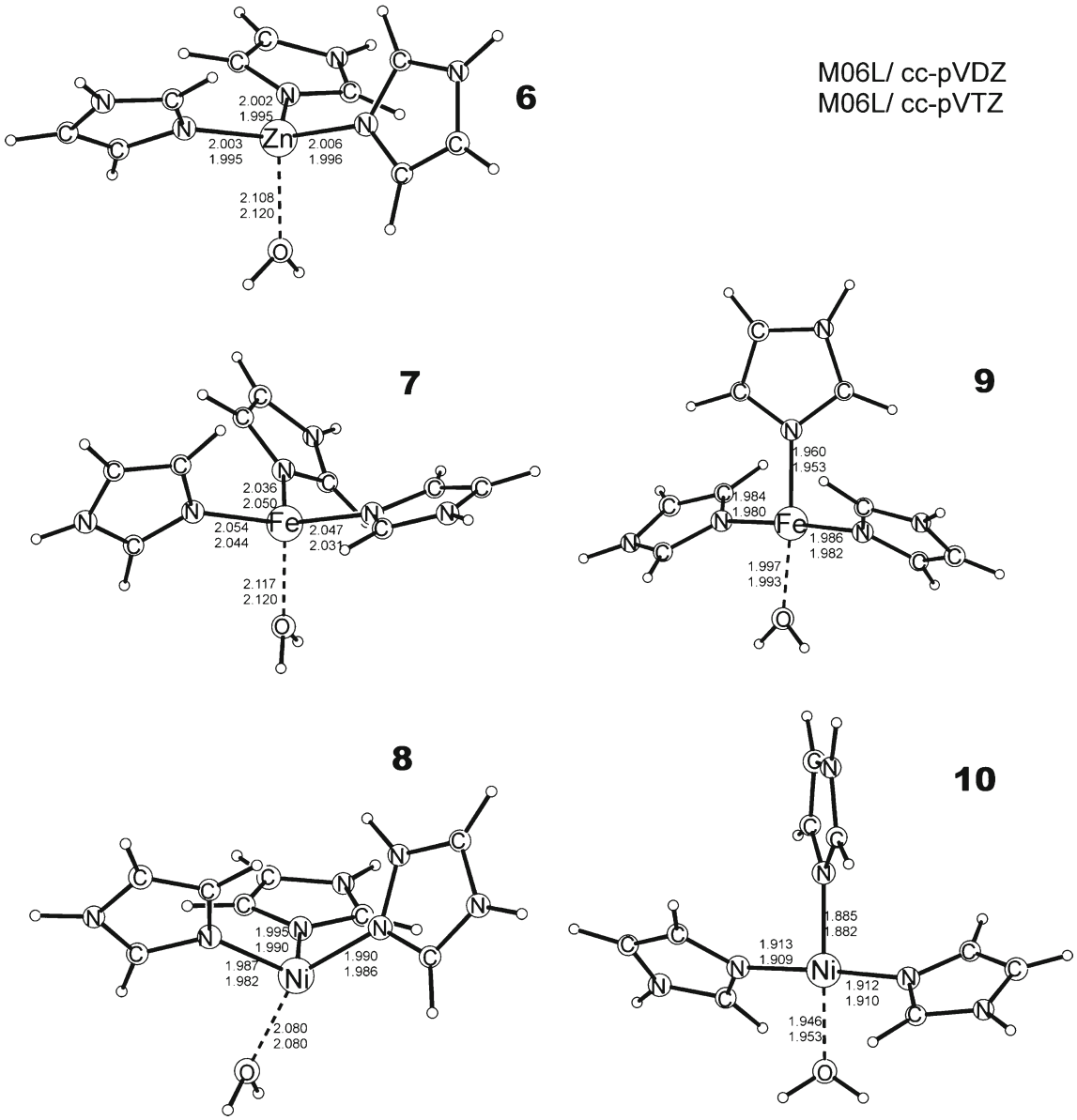

Fig. 2 Equilibrium structures (bond lengths in Å) of metalloproteases active site models with imidazole ligands

Table 1 ZPVE corrected energy difference (ΔH_0) between the high and low spin states of the enzyme active site models $[R_3M\text{-}OH_2]^{2+}$ (R=NH_3, $C_3N_2H_4$; M=Fe, Ni)

M	B3LYP		M06L		MP2
	cc-pVDZ	cc-pVTZ	cc-pVDZ	cc-pVTZ	cc-pVDZ
R=NH_3					
Fe	−23.2	−22.2	−28.1	−26.5	−48.3
Ni	−8.0	−6.4	−7.2	−5.6	−21.3
R=$C_3N_2H_4$					
Fe	−19.3	−18.5	−21.8	−20.4	—
Ni	−3.5	−2.4	−3.6	−2.2	—

simple model of an inhibitor containing the silanediol functionality). These complexes are compared with analogous complexes with N-acetylhydroxylamine as one of the most potent inhibitor with hydroxamic functionality.

Computational methods

Geometries of stationary points have been fully optimized and characterized by harmonic vibrational frequency calculations using the B3LYP [47, 48] and M06L [49] density functional methods. The latter functional was reported to have the best overall performance of any functional (including the popular B3LYP) for the study of organometallic thermochemistry and noncovalent interactions [50–54]. For smaller systems, in which amino acid residues were modeled by ammonia molecules, second-order Moller-Plesset perturbation theory (MP2) with the frozen core approximation [55] was also used. In order to account for long range dispersion forces, DFT-D3 [56] program has been used to correct the calculated energies (B3LYP/cc-pVTZ) in larger systems. The Dunning correlation-consistent sets [57] were employed. All the methods and basis sets were used as implemented in the Gaussian09 program [58]. In the DFT methods the integration was carried out with the Int=Ultrafine option and, for all the methods employed,

Table 2 Gibbs free energies (ΔG_{298}) of the reaction $[R_3M\text{-}OH_2]^{2+}$ + MBG → $[R_3M\text{-}MBG]^{2+}$ + H_2O

	MBG	spin state	B3LYP			M06L		MP2
			cc-pVDZ	cc-pVTZ	cc-pVDZDFT-D3 corrected	cc-pVDZ	cc-pVTZ	cc-pVDZ
R=NH_3	M=Zn							
	HAM	singlet	−20.8	−22.9	—	−22.5	−24.5	−22.1
	DMSD	singlet	−15.7	−14.8	—	−20.6	−19.3	−18.7
	M=Fe							
	HAM	triplet	−26.5	−27.7	—	−30.7	−29.5	−30.8
	DMSD	triplet	−22.8	−19.8	—	−29.9	−33.7	−32.4
	HAM	quintet	−24.6	−26.1	—	−27.4	−28.4	−25.6
	DMSD	quintet	−20.7	−17.8	—	−26.5	−23.6	−24.5
	M=Ni							
	HAM	singlet	−24.6	−25.4	—	−28.3	−28.1	−26.6
	DMSD	singlet	−18.9	−17.1	—	−23.1	−21.3	−21.5
	HAM	triplet	−26.1	−26.5	—	−29.4	−31.7	−28.1
	DMSD	triplet	−25.9	−23.0	—	−31.8	−28.5	−29.2
R=$C_3N_2H_4$	M=Zn							
	HAM	singlet	−10.8	−11.6	−16.9	−15.4	−15.0	—
	DMSD	singlet	−6.9	−5.8	−14.0	−12.1	−10.0	—
	M=Fe							
	HAM	triplet	−13.2	−13.6	−18.7	−19.7	−20.3	—
	DMSD	triplet	−7.2	−4.8	−13.3	−16.1	−13.9	—
	HAM	quintet	−12.5	−13.1	−18.2	−16.8	−16.9	—
	DMSD	quintet	−7.2	−6.0	−13.9	−13.5	−11.9	—
	M=Ni							
	HAM	singlet	−11.0	−13.0	−18.3	−16.1	−16.5	—
	DMSD	singlet	−5.3	−4.4	−13.3	−11.6	−9.9	—
	HAM	triplet	−15.0	−14.7	−20.6	−19.9	−21.5	—
	DMSD	triplet	−12.0	−9.2	−17.9	−18.6	−16.8	—

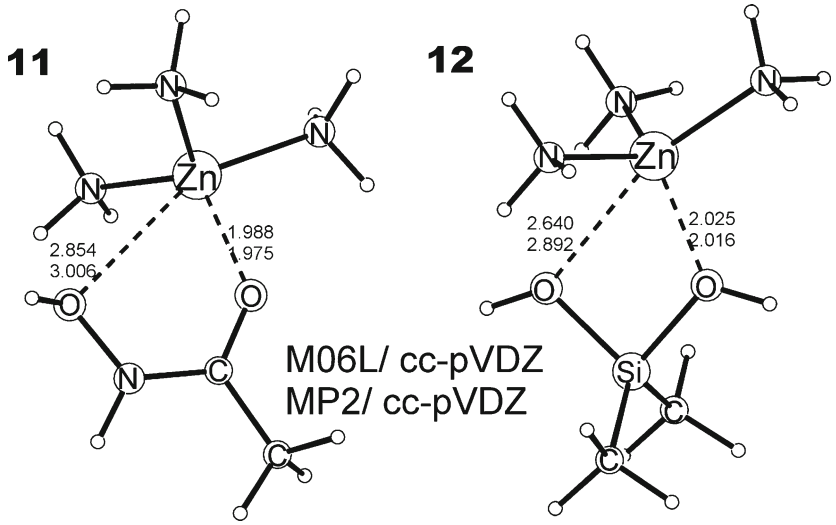

Fig. 3 Equilibrium structures (bond lengths in Å) of the products of the water displacement reaction $[(NH_3)_3Zn\text{-}OH_2]^{2+}$ + MBG → $[(NH_3)_3Zn\text{-}MBG]^{2+}$ + H_2O for MBG = HAM, DMSD

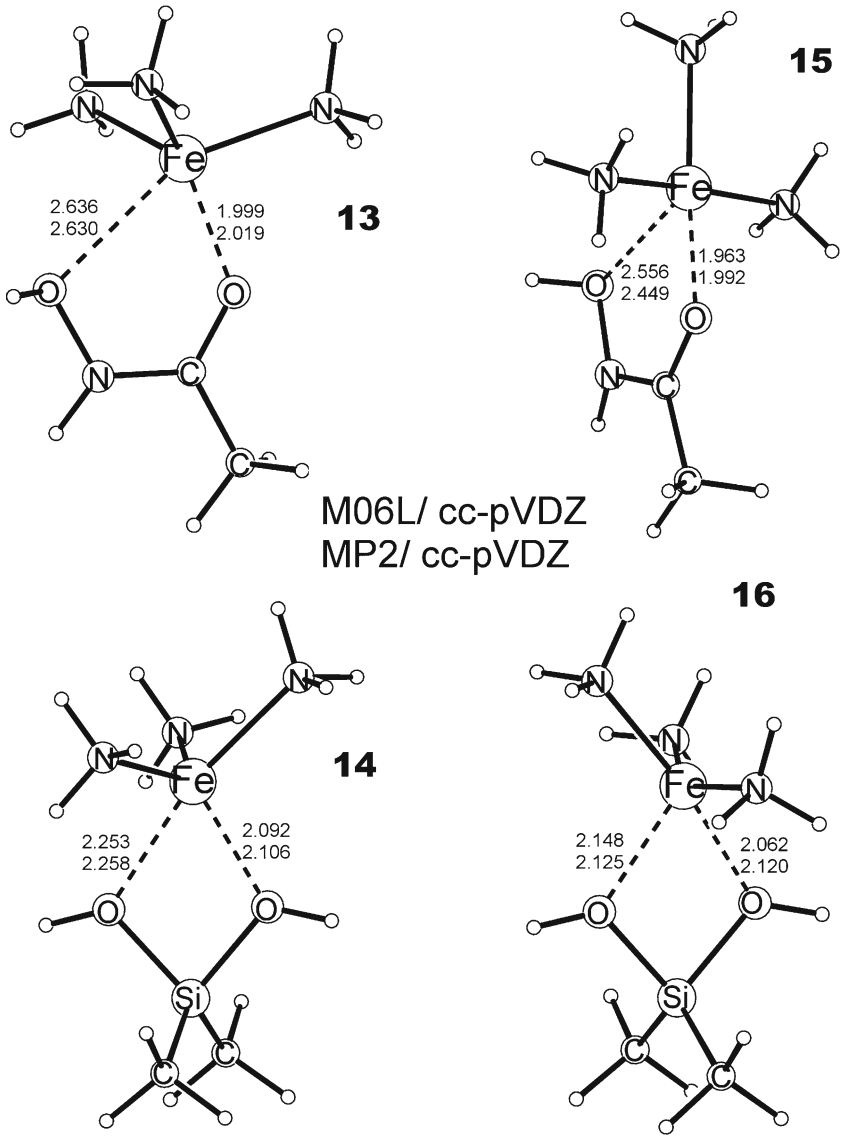

Fig. 4 Equilibrium structures (bond lengths in Å) of high spin (**13**, **14**) and low spin (**15**, **16**) states of the products of the water displacement reaction $[(NH_3)_3Fe\text{-}OH_2]^{2+}$ + MBG → $[(NH_3)_3Fe\text{-}MBG]^{2+}$ + H_2O for MBG=HAM, DMSD

the geometry optimization criterion used were those corresponding to the Gaussian09 Opt=Tight option. Natural bond orbital (NBO) [59] calculations were accomplished using the program NBO v3.1 [60] as implemented in Gaussian 09.

Results and discussion

Models of the enzyme active site

Equilibrium structures of two models of Zn^{2+}, Fe^{2+}, and Ni^{2+} containing enzymes are presented in Figs. 1 and 2. In the first model, the three amino acid residues are replaced by ammonia molecules, while in the second one they are replaced by an imidazole ring which mimics a histidine residue, which is a common coordinating ligand in different metalloproteins.

Each of these two models has its own advantages and drawbacks. The ammonia model allows one to use more sophisticated quantum chemical methods, while the imidazole model is closer to the reproduction of steric hindrances around the metal cation in real metalloproteases.

Ammonia complexes of zinc (**1**, Fig. 1) as well as the high spin states of Fe^{2+} and Ni^{2+} complexes (**2** and **3**, Fig. 1) have structures with symmetry close to C_s. In the Zn^{2+} complex the position of the water molecule depends on the basis set, i.e., in structures optimized with the double-z set it intersects the symmetry plane, while in those with triple-z set it lies in the plane. The difference between the in-plane and out-of-plane Zn-N bonds also depends on the basis set employed: for cc-pVDZ two out-of-plane Zn-N bonds are slightly longer than the in-plane bond and for structures optimized with cc-pVTZ set the order is inverse (Fig. 1).

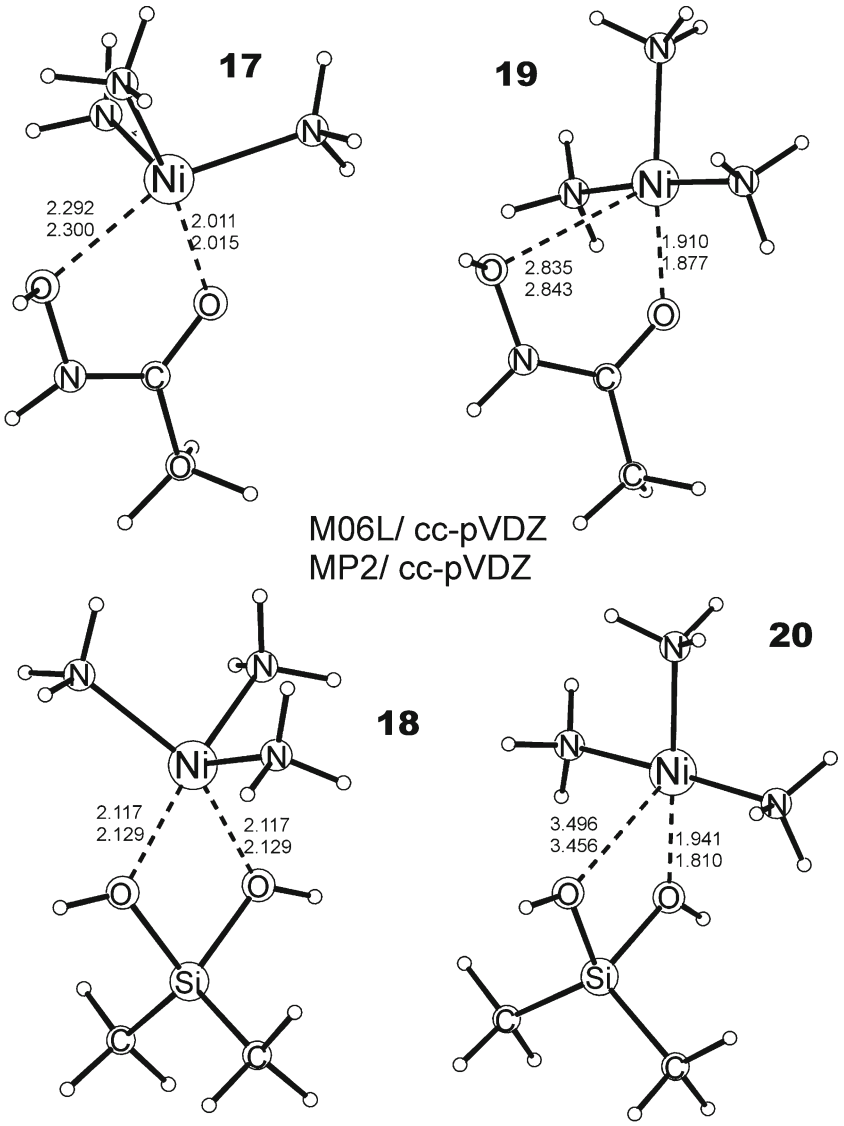

Fig. 5 Equilibrium structures (bond lengths in Å) of high spin (**17**, **18**) and low spin (**19**, **20**) states of the products of the water displacement reaction $[(NH_3)_3Ni\text{-}OH_2]^{2+}$ + MBG → $[(NH_3)_3Ni\text{-}MBG]^{2+}$ + H_2O for MBG=HAM, DMSD

In the optimized structures of the high spin Fe^{2+} complex (**2**) no such difference was detected: in all structures the water molecule intersects the symmetry plane and in-plane Fe-N bonds are shorter.

The similar position of water was found in optimized structures of the Ni complex, although in this case the in-plane Ni-N bonds are substantially longer that those out-of-plane. The other feature which was not observed in Zn^{2+} and Fe^{2+} complexes is that the water molecule substantially deviates from the axis of the $(NH_3)_3Ni^{2+}$ moiety. This deviation may be characterized as a difference between in-plane and out-of-plane O-M-N bond angles (θ=δO-M-N1—δO-M-N2). This value in the zinc complex (**1**, Fig. 1) is close to zero. In the high spin state of the $[(NH_3)_3Fe\text{-}OH_2]^{2+}$ complex its value is also small, while for the nickel complex (**3**, Fig. 1) it reaches 47°.

Low spin states of the complexes $[(NH_3)_3Fe\text{-}OH_2]^{2+}$ (**4**, triplet) and $[(NH_3)_3Ni^{2+}\text{-}OH_2]$ (**5**, singlet) have a square planar arrangement of ligands [36]. This difference in the structure of low and high spin states of transition metal complexes was rationalized by Dobbs et al. [36] as resulting from the dramatic destabilization of the highest of the singly occupied molecular orbitals (SOMOs) occurring when the tetrahedron flattens. This orbital is not occupied in low spin states of these complexes and, therefore, the square planar structure is more stable. The NBO analyses of the high spin states of iron (**2**) and nickel (**3**) complexes show that the SOMOs responsible for their structures have different configurations. In **2** it has a large contribution of d_{Z^2} electrons of Fe, while the highest SOMO of **3** is populated by the Ni d_{YZ} electron. This difference in the symmetry of the SOMO may lead to the different destabilization of this orbital on going from the tetrahedral to the square planar configuration. Due to this difference the triplet state of the $[(NH_3)_3Ni\text{-}OH_2]^{2+}$ complex has a significant deviation from the tetrahedral arrangement toward the square planar one. Note also that the energy difference between the high and low spin states of Ni complexes is substantially lower than that for Fe complexes (Table 1).

Energy minima for low spin states of both Fe^{2+} (**4**) and Ni^{2+} (**5**) complexes obtained at different levels of theory has exact (B3LYP, MP2 for Fe^{2+}) or approximate C_s symmetry. However, the position of the water molecule differs in Fe^{2+} and Ni^{2+} complexes: in **4** it lies in the symmetry plane of the molecule, while in **5** it intersects this plane.

Similar complexes were found for the model with imidazole ligands (**6**–**10**, Table 2). More bulky imidazole substituents and the minimization of the repulsion between these rings result in the absence of even approximate symmetry elements in their equilibrium structures.

Computational problems connected with the substantially larger number of atoms in the imidazole model allowed us to use only DFT methods for their optimization. Nevertheless, the comparison of equilibrium bond lengths (Fig. 1) indicates that the M06L method gives results which are close to those of MP2 which may be considered as the most reliable quantum chemical method employed.

M-O bond distances in imidazole complexes are slightly longer than analogous equilibrium bond lengths in ammonia complexes. Note, also, that the energy difference between the high and low spin Ni^{2+} complexes substantially diminishes on going to imidazole complexes (Table 1)

Complexes modeling the interaction between the active site and the MBGs

Equilibrium structures of $(NH_3)_3M^{2+}$ complexes with N-acetylhydroxylamine ($CH_3C(=O)NH(OH)$, henceforth denoted as HAM), as a model of one of the strongest MBG [36], and dimethylsilanediol ($((CH_3)_2Si(OH)_2$, from now on denoted as DMSD), as a model of the silanediol based protease inhibitors, are depicted in Figs. 3–5 (**11**–**20**). Further, the binding ability of these groups are estimated as the Gibbs free energy of the $[R_3M\text{-}OH_2]^{2+}$ + MBG → $[R_3M\text{-MBG}]^{2+}$ + H_2O water replacement reactions. These values, calculated with the different methods used, are reported in Table 2.

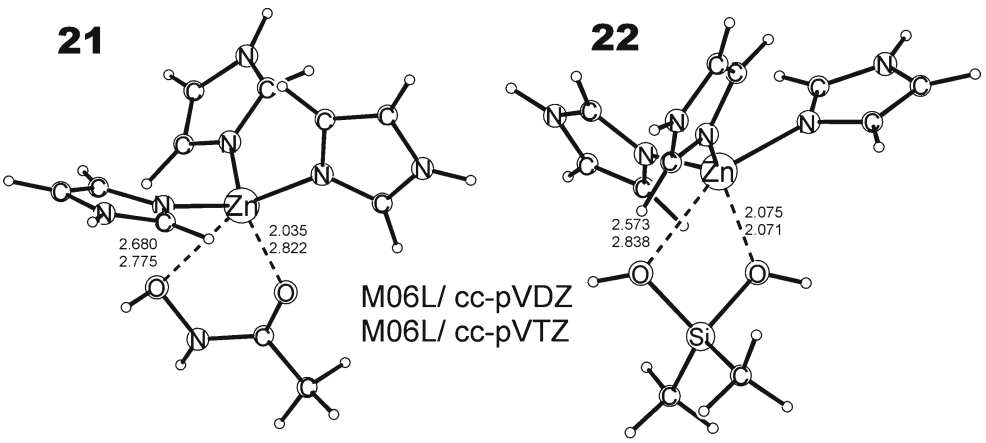

Fig. 6 Equilibrium structures (bond lengths in Å) of the products of the water displacement reaction $[(H_4C_3N_2)_3Zn\text{-}OH_2]^{2+}$ + MBG → $[(H_4C_3N_2)_3Zn\text{-MBG}]^{2+}$ + H_2O for MBG = HAM, DMSD

The complex formed by the $(NH_3)_3Zn^{2+}$ cation and the HAM molecule demonstrates a feature revealed in previous theoretical works and considered there as unexpected [36–46]. This is a monodentate chelation of the hydroxamic functionality through the formation of a single dative bond between the carbonyl oxygen of the binding group and the metal of the model system. This is in contrast to the bidentate chelation of the inhibitor hydroxamates to the Zn^{2+} cation observed in the X-ray studies of histone deacetylases [5, 7]. Our optimized structure of the complex with HAM, $[(NH_3)_3Zn\text{-HAM}]^{2+}$ (**11**, Fig. 3), also demonstrate the monodentate binding: Zn…O=C interatomic distance (MP2/cc-pVDZ) is in the 1.975 Å while the Zn…OH distance is 3.006 Å (Fig. 3).

Monodentate binding is also observed in the DMSD complex (**12**, Fig. 3). However, differences between shorter and longer Zn…OH contacts are smaller. In the MP2 method these interatomic distances are 2.016 and 2.892 Å correspondingly.

High spin states (quintet) of Fe^{2+} complexes have structures similar to those of zinc analogues (**13** and **14**, Fig. 4). In the equilibrium structure of the HAM complex (**13**) the Fe…O=C distance is also substantially shorter than the Fe…OH distance. Nevertheless, in the DMSD complex (**14**) the difference between two Fe…OH bond lengths is significantly smaller than in the analogous complex with zinc (**12**, Fig. 3). In the low spin state, i.e., triplet (**15**, Fig. 4) as in the water complex (**4**, Fig. 1) a square planar arrangement of ligands occurs with a shorter Fe…O=C contact. In contrast, in the triplet state of the DMSD complex the planar arrangement of the $(NH_3)_3Fe^{2+}$ moiety is seriously distorted due to the fact that both Fe…OH bonds are almost equal (**16**, Fig. 4).

In the Ni^{2+} complexes (**17**–**20**, Fig. 5) the tendency for the growth of the bidentate character of chelation continues for the high spin (triplet) states: the DMSD complex (**18**) belongs to the C_s symmetry point group with equal Ni…OH distances. Nonetheless, the low spin (singlet) states of both HAM (**19**) and DMSD (**20**) complexes are distinctly monodentate, in contrast to their iron analogs (**15** and **16**, Fig. 4).

Equilibrium structures of complexes modeled using the Zn^{2+} cation and three imidazole rings, $(C_3N_2H_4)_3Zn^{2+}$, to mimic the enzyme active site and both HAM (**21**) and DMSD (**22**) as MBGs are depicted in Fig. 6. As can be seen, they have the same pattern of metal binding that the

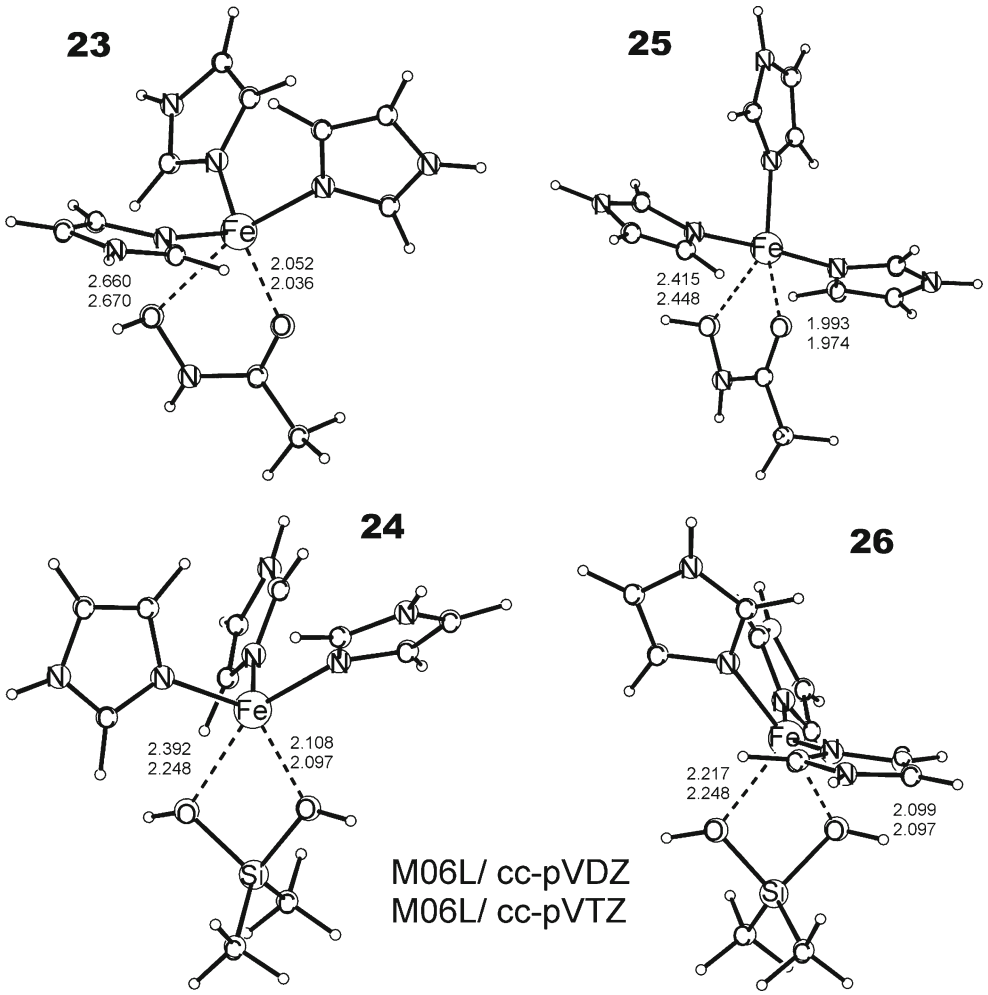

Fig. 7 Equilibrium structures (bond lengths in Å) of high spin (**23**, **24**) and low spin (**25**, **26**) states of the products of the water displacement reaction $[(H_4C_3N_2)_3Fe\text{-}OH_2]^{2+}$ + MBG → $[(H_4C_3N_2)_3Fe\text{-MBG}]^{2+}$ + H_2O for MBG=HAM, DMSD

abovementioned ammonia models (Fig. 3). However, the difference between Zn…O distances slightly decrease. This tendency cannot be traced in imidazole complexes of Fe (**23**–**26**, Fig. 7) and Ni (**27**–**30**, Fig. 8). In general, M…O bond distances in imidazole complexes are longer than in the corresponding ammonia complexes.

Binding abilities of the MBGs

The slightly weaker bonding in the imidazole model manifests in the lower energies calculated for the reaction $[R_3M\text{-}OH_2]^{2+}$ + MBG → $[R_3M\text{-}MBG]^{2+}$ + H_2O. This reaction is used as a measure of the binding ability of different MBGs [36]. In the analysis of the data we will focus on the comparison between binding ability of one of the strongest binder, which is HAM, and DMSD (Table 2). Gibbs free energies of the water replacement reaction are used as characteristics of binding ability.

Three quantum chemical methods were used for the estimation of these values: DFT functionals B3LYP and M06L (with cc-pVDZ and cc-pVTZ basis sets), and, only for ammonia complexes, *ab initio* MP2 method with the cc-pVDZ basis set. Since MP2 method may be considered as the most reliable we may judge the performance of DFT methods as they imitate the MP2 results. From this point of view M06L gives closer to MP2 energies (Table 2), while B3LYP slightly underestimates binding energies. Noticeably, DFT-D3 dispersion correction of the B3LYP/cc-pVTZ Gibbs free energies (calculated for those systems which size prevented running MP2 calculations) bring the calculated values close to M06L/cc-pVTZ values (Table 2).

For M=Zn the silanediol group is only by 2 kcal mol^{-1} a weaker binder than HAM. All methods (for the ammonia and imidazole models) predict that both HAM and DMSD exhibit stronger binding for the low spin state of the iron cation (triplet) than for its high spin state (quintet). Note, that the binding abilities estimated with MP2 and M06L methods and the cc-pVDZ basis set for the silanediol group are higher in the triplet state and nearly equal in the quintet state when compared to values calculated for the HAM complexes. In contrast to this, B3LYP predicts substantially stronger binding of HAM in both triplet and quintet states.

For $[(NH_3)_3Ni\text{-}MBG]^{2+}$ complexes, all methods predict higher binding in the high spin (triplet) state. In this state, DMSD appear to be a slightly better binder than HAM,

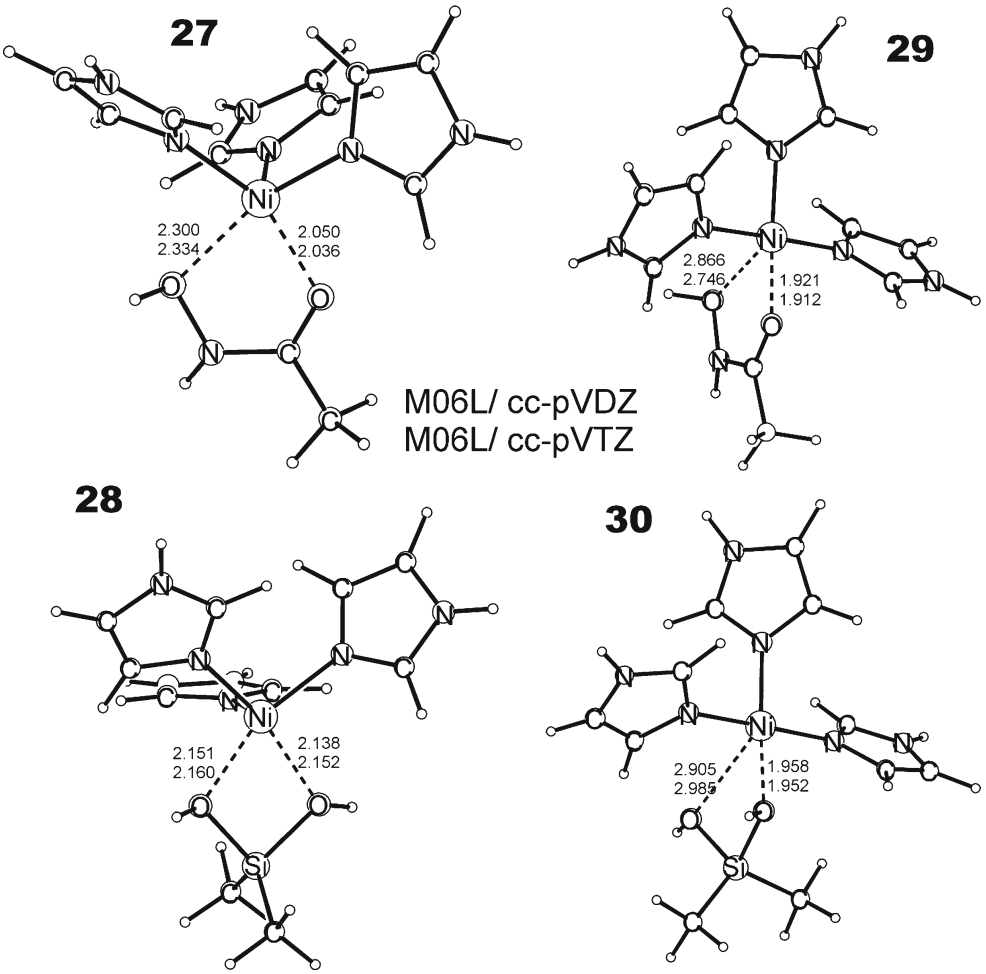

Fig. 8 Equilibrium structures (bond lengths in Å) of high spin (**27**, **28**) and low spin (**29**, **30**) states of the products of the water displacement reaction $[(H_4C_3N_2)_3Ni\text{-}OH_2]^{2+}$ + MBG → $[(H_4C_3N_2)_3Ni\text{-}MBG]^{2+}$ + H_2O for MBG=HAM, DMSD

according to MP2 and M06L results, while in the singlet state HAM is preferred (Table 2).

In general, the order of binding ability for the silanediol group, i.e., $Fe^{2+}(t) > Ni^{2+}(t) > Fe^{2+}(q) > Ni^{2+}(s) > Zn^{2+}$ in ammonia models, is close to that in HAM models, which differs only in the relative values for $Fe^{2+}(q)$ and $Ni^{2+}(s)$. DMSD shows the predominance of $Fe^{2+}(q)$, while for HAM complexes these values are almost equal. However, in imidazole models the order is slightly different. Here the binding ability of HAM and silanediol functionalities for $Ni^{2+}(t)$ complexes is higher than those for Fe^{2+}.

Intermediates in the water displacement reaction

In previous theoretical studies of the interaction between metal complexes and inhibiting molecules the intermediate in the reaction of the water displacement were not regarded. Since transition metal cations may increase their coordination up to six ligands [61–64], one may conclude that the complex formed by the attack of MBG on $[R_3M\text{-}OH_2]^{2+}$ should be an energy minimum rather than a transition state. Indeed, complexes of HAM (**31**–**32**) and DMSD (**33**–**34**) with the ammonia $[(NH_3)_3Zn\text{-}OH_2]^{2+}$ model of a Zn-enzyme active site (Fig. 9) are minima on their potential energy surfaces. There are two modifications of these complexes; one which is formed by the back-side attack of the MBG on the $[(NH_3)_3Zn\text{-}OH_2]^{2+}$ complex (**31**, **33**), the other by the front-side attack (**32**, **34**). Note, that these two types of complexes may be realized only for complexes with small ammonia ligands. However, as discussed below, only one type of complex exists in the models with more bulky imidazole ligands.

The back-side complexes (**31**, **33** Fig. 9) originate from the attack of the MBG on **1** (Fig. 1) from the side opposite to a water molecule. It has a trigonal bipyramidal structure with a pentacoordinated zinc atom. The coordination of both HAM and DMSD is obviously monodentate (the second Zn…O interatomic distance is over 3 Å). However, in the

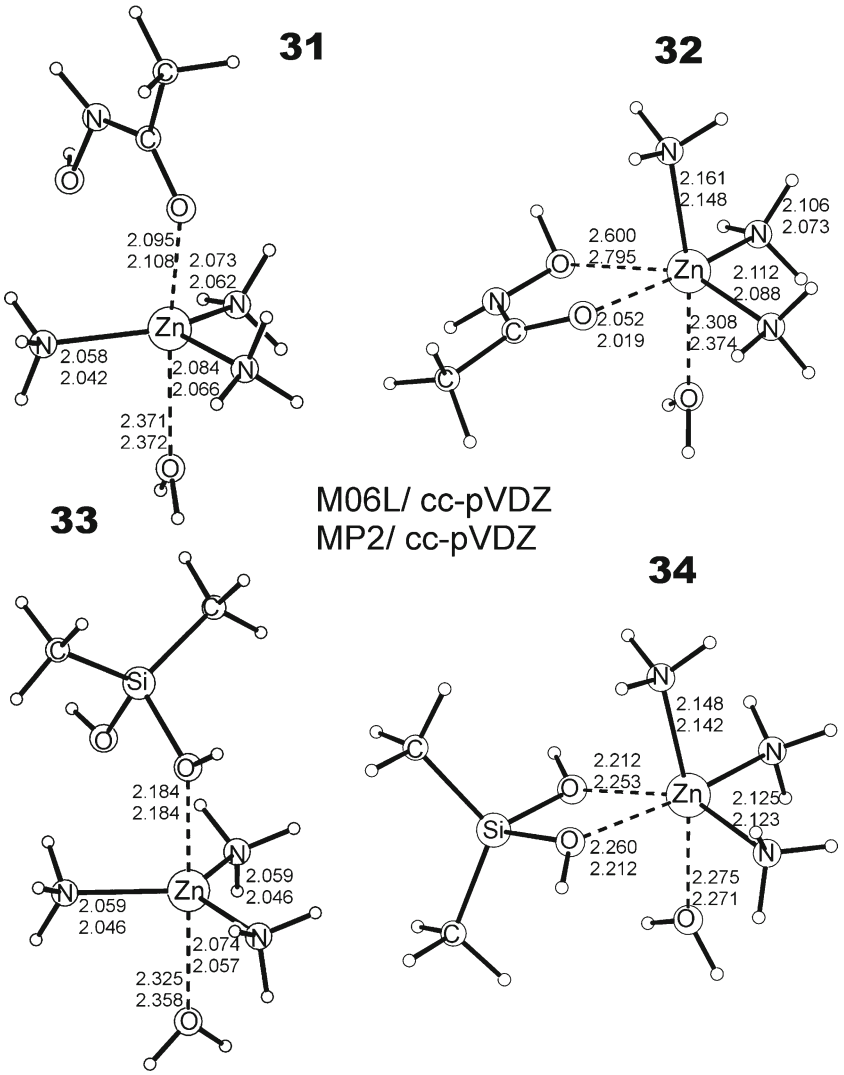

Fig. 9 Equilibrium structures (bond lengths in Å) of the intermediates in the back-side (**31**, **33**) and front-side (**32**, **34**) attack of the MBG in the water displacement reaction $[(NH_3)_3Zn\text{-}OH_2]^{2+} + MBG \rightarrow [(NH_3)_3Zn\text{-}MBG]^{2+} + H_2O$ for MBG=HAM, DMSD

front-side HAM complex (**32**) Zn…O interatomic distances are more equal and the structure looks like distorted octahedron. Zn…O bonds become almost equivalent in the DMSD complex (**34**). Despite the quite different structures of back-side and front-side complexes, the difference in energies between them is very small (Table 3).

Analogous complexes for the quintet state of iron (**35**–**38**, Fig. 10) have noticeably higher bidentate character of Fe…O bonding. Even for the HAM complexes the difference in Fe…O bonds do not exceed 0.4 Å (MP2 results), while for the DMSD complexes this difference is below 0.1 Å. All the structures have the shape of a distorted octahedron, only in the case of back-side complexes a water molecule and a short Fe…O bond to a MBG group are in axial positions (**35**,**37**), while for front-side complexes (**36**, **38**) these axial positions are occupied by the water molecule and one of the ammonia ligands. The energy differences between back-side and front-side complexes are also small, but in contrast to the zinc analogues the front-side complexes of Fe have slightly lower energies.

Equilibrium structures of the complexes of the triplet state of $[(NH_3)_3Fe\text{-}OH_2]^{2+}$ with HAM (**39**) and DMSD (**40**) are depicted in Fig. 11. They have the form of a distorted octahedron, similar to the analogous high spin structures **35** and **37**. Their complexation energies, as for other low spin state complexes, are by ca. 10 kcal mol^{-1} higher (Table 3).

The triplet state of the $[(NH_3)_3Ni\text{-}OH_2]^{2+}$ complex (**41**, Fig. 12) formed by the back-side attack of HAM has a distorted trigonal bipyramidal structure and is bound to HAM in a monodentate fashion, similarly to the analogous complex of zinc (**31**, Fig. 9). However, the second complex (**42**) has a bidentate bonding to HAM oxygen atoms and an octahedral structure. It is more stable than **41** by ca. 6 kcal mol^{-1} (Table 3).

Both complexes of DMSD (**43** and **44**) have octahedral structure and bidentate bonding. Complex **44** is a nearly perfect octahedron. Note, that due to rather short and almost equal Ni-N and Ni…O distances, equilibrium bond lengths optimized in M06L and MP2 methods are nearly equal. This

Table 3 Energies (kcal mol^{-1}) of the formation of the complex between $[R_3M\text{-}OH_2]^{2+}$ and MBGs estimated by M06L and MP2 methods with cc-pVDZ basis set

	MBG (attack) nº in Figs. 9–13	Spin state	M06L/cc-pVDZ			MP2/cc-pVDZ		
			ΔE_e	ΔE_0	ΔG_{298}	ΔE_e	ΔE_0	ΔG_{298}
$R=NH_3$	M=Zn							
	HAM (back) 31	singlet	−47.2	−46.3	−33.3	−46.2	−45.2	−33.1
	HAM (front) 32	singlet	−46.3	−45.8	−33.0	−44.9	−44.0	−31.6
	DMSD (back) 33	singlet	−46.0	−44.5	−30.9	−43.8	−42.5	−29.5
	DMSD (front) 34	singlet	−45.8	−44.7	−30.4	−41.7	−41.4	−28.8
	M=Fe							
	HAM (back) 35	quintet	−51.7	−51.5	−40.6	−52.1	−51.4	−40.1
	HAM (front) 36	quintet	−54.0	−53.9	−42.5	−53.4	−52.7	−41.3
	DMSD (back) 37	quintet	−53.0	−52.8	−40.5			
	DMSD (front) 38	quintet	−53.1	−52.8	−41.5			
	HAM 39	triplet	−61.8	−61.3	−49.6	−62.4	−62.3	−50.8
	DMSD 40	triplet	−58.4	−58.2	−46.5			
	M=Ni							
	HAM (back) 41	triplet	−56.3	−55.2	−43.0	−55.4	−54.1	−42.0
	HAM (front) 42	triplet	−62.5	−61.2	−47.9	−61.2	−60.1	−47.4
	DMSD (back) 43	triplet	−61.1	−60.0	−46.0	−58.6	−58.0	−51.2
	DMSD (front) 44	triplet	−62.1	−60.9	−47.3	−59.2	−58.4	−52.2
$R=C_3N_2H_4$	M=Zn							
	HAM 45	singlet	−34.0	−33.2	−21.1	—	—	—
	DMSD 46	singlet	−31.5	−30.9	−17.9	—	—	—
	M=Fe							
	HAM 47	quintet	−38.6	−37.5	−23.6	—	—	—
	DMSD 48	quintet	−38.1	−37.3	−23.5	—	—	—
	M=Ni							
	HAM 49	triplet	−46.9	−45.5	−31.6	—	—	—
	DMSD 50	triplet	−45.5	−44.3	−30.1	—	—	—

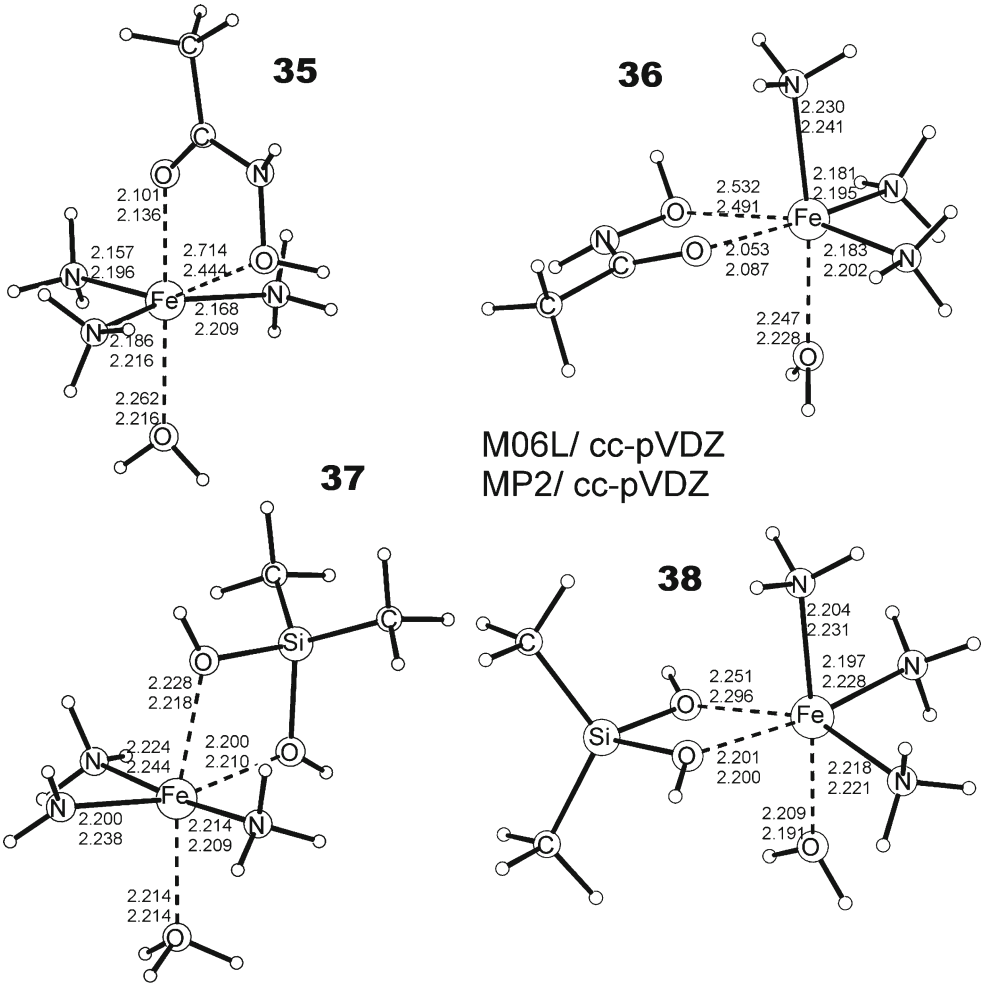

Fig. 10 Equilibrium structures (bond lengths in Å) of high spin states (quintet) of the intermediates in the in the back-side (**35**, **37**) and front-side (**36**, **38**) attack of the MBG in the water displacement reaction $[(NH_3)_3Fe\text{-}OH_2]^{2+}$ + MBG → $[(NH_3)_3Fe\text{-}MBG]^{2+}$ + H_2O for MBG=HAM, DMSD

complex also has the highest complexation energy among all the intermediate complexes studied. All attempts to find a penta- or hexacoordinated intermediates for the attack of both HAM and DMSD molecules on the $[(NH_3)_3Ni\text{-}OH_2]^{2+}$ singlet complex (similar to analogous complexes for the low spin state of iron, structures **39** and **40**) failed. Structures converge to complexes **19** and **20** (Fig. 5) with a water molecule hydrogen bonded to ammonia ligands.

In complexes with bulky imidazole ligands, the possibility of different ways of the attack is sterically restricted. Therefore, only one type of intermediate complex was found for tetrahedral models. All complexes may be described as a distorted octahedron. In the zinc complex (**45**, Fig. 13) the oxygen atoms of the water molecule and the carbonyl group of HAM are in axial positions, while the nitrogen atoms of the imidazole rings and the HAM hydroxyl oxygen may be

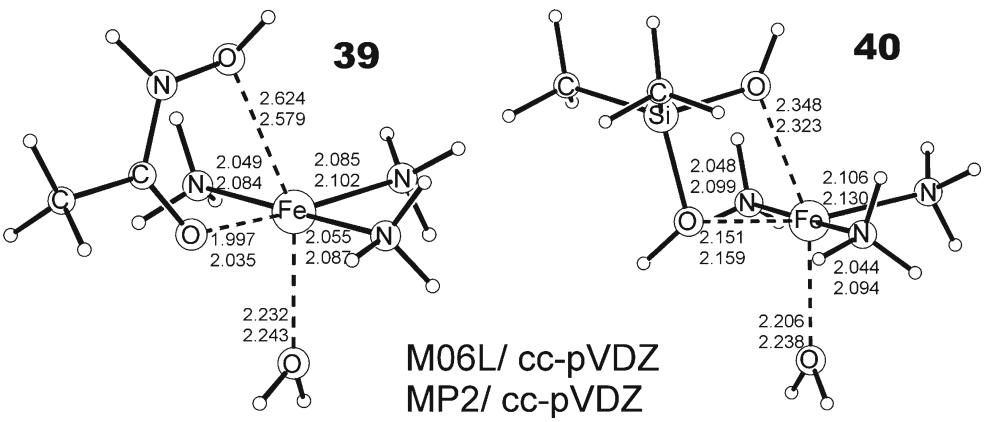

Fig. 11 Equilibrium structures (bond lengths in Å) of low spin states (triplet) of the intermediates in the water displacement reaction $[(NH_3)_3Fe\text{-}OH_2]^{2+}$ + MBG → $[(NH_3)_3Fe\text{-}MBG]^{2+}$ + H_2O for MBG=HAM, DMSD

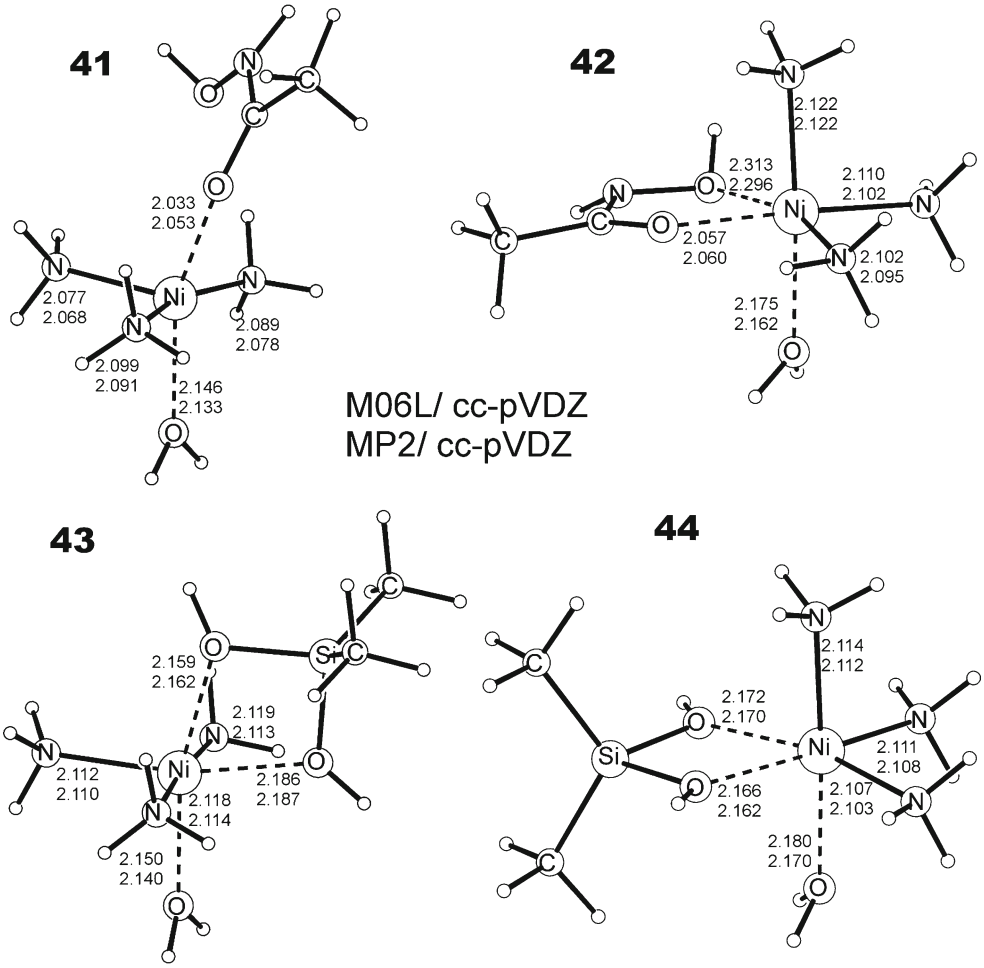

Fig. 12 Equilibrium structures (bond lengths in Å) of high spin states (triplet) of the intermediates in the in the back-side (**41**, **43**) and front-side (**42**, **44**) attack of the MBG in the water displacement reaction $[(NH_3)_3Ni\text{-}OH_2]^{2+}$ + MBG → $[(NH_3)_3Ni\text{-}MBG]^{2+}$ + H_2O for MBG=HAM, DMSD

assigned to equatorial positions despite the rather large Zn…O distance of the latter. In the octahedral complex with the silanediol group (**46**) the bonding is completely bidentate.

The bidentate character of bonding of HAM is increasing in Fe (**47**, Fig. 14) and Ni (**49**, Fig. 14) complexes. These complexes as well as the analogous complexes with DMSD (**48**, **50**) have octahedral structure. Formation energies of imidazole complexes are lower than corresponding ammonia complexes, but the difference between energies of complexes with HAM and DMSD remains unchanged with those for DMSD being a few kcal mol^{-1} lower than those for HAM complexes.

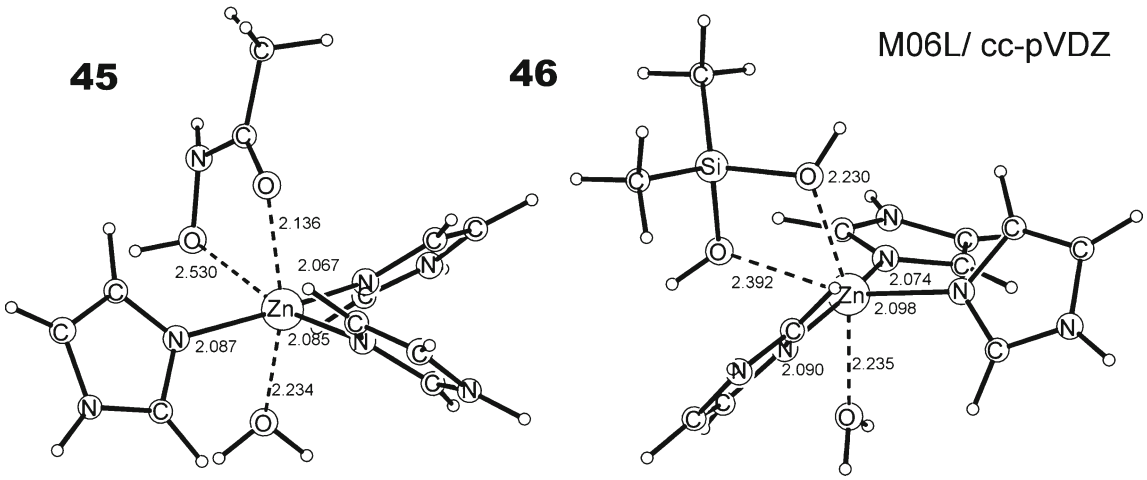

Fig. 13 Equilibrium structures (bond lengths in Å) of the intermediates in the water displacement reaction $[(H_4C_3N_2)_3Zn\text{-}OH_2]^{2+}$ + MBG → $[(H_4C_3N_2)_3Zn\text{-}MBG]^{2+}$ + H_2O for MBG=HAM, DMSD

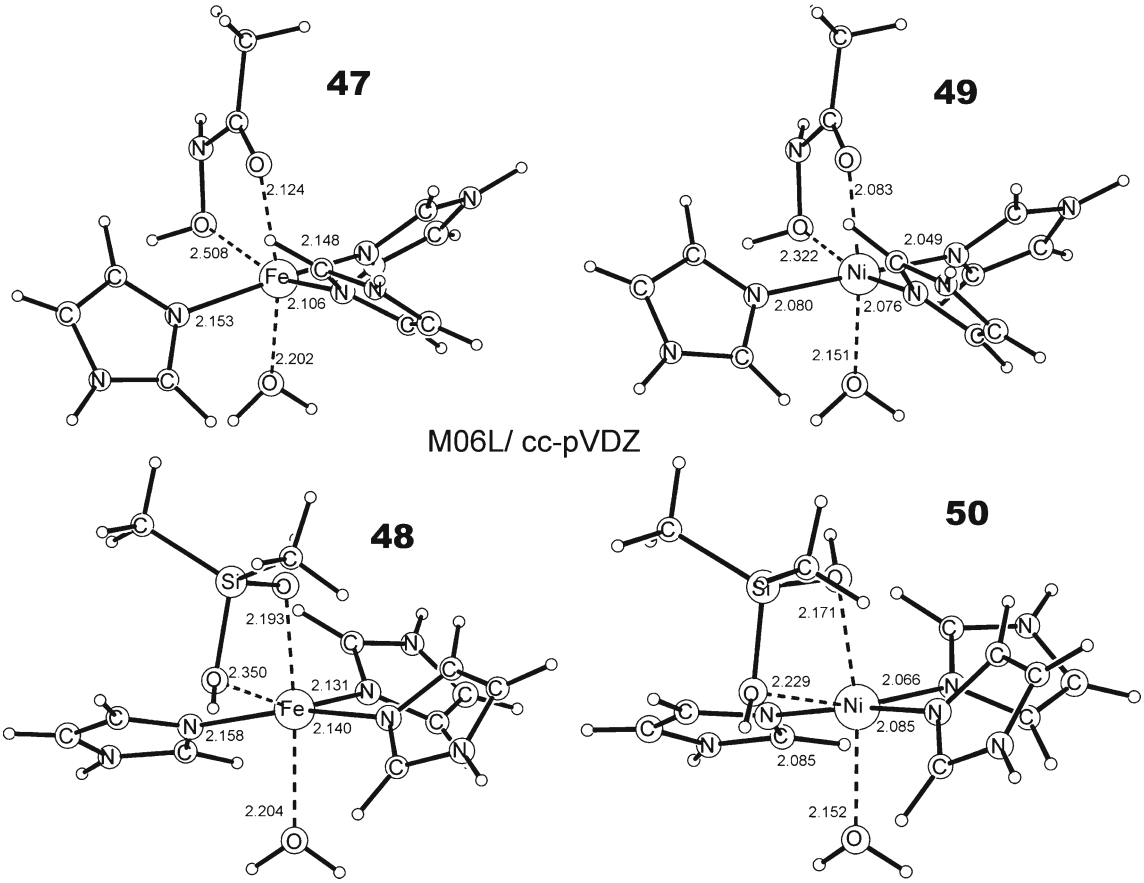

Fig. 14 Equilibrium structures (bond lengths in Å) of the high spin states of the intermediates in the water displacement reaction $[(H_4C_3N_2)_3M\text{-}OH_2]^{2+}$ + MBG → $[(H_4C_3N_2)_3M\text{-MBG}]^{2+}$ + H_2O for M=Fe, Ni and MBG=HAM, DMSD

Conclusions

1. Enzymes are modeled by the tridentate complexes of Zn^{2+}, Fe^{2+} and Ni^{2+} metal dications with an exchangeable water molecule in which amino acid residues are mimicked by (i) ammonia and (ii) imidazole ligands. The inhibiting activity of the silanediol functionality is compared to that of hydroxamic acids (HAM) by the calculation of the energies of the water displacement reaction by metal binding groups $[R_3M\text{-}OH_2]^{2+}$ + MBG → $[R_3M\text{-MBG}]^{2+}$ + H_2O, where R=NH_3 and $C_3N_2H_4$, M=Zn, Fe, Ni.
2. The equilibrium geometries of the $[R_3Zn\text{-}OH_2]^{2+}$ complexes and the high spin states of the iron and nickel analogous are characterized by their distorted tetrahedral structure in which the water molecule lies on the axis of the R_3M^{2+} group for R=Zn and Fe, but substantially deviates from this axis for R=Ni. Low spin states of iron and nickel complexes have a square planar arrangement of ligands.
3. Distances between the metal atom and oxygen atoms of HAM as well as of silanediol are quite different for $[R_3Zn\text{-HAM}]^{2+}$ complexes (monodentate binding) but become more equal on going to the high spin states of iron and nickel (bidentate binding).
4. The comparison of the different quantum chemical methods employed for the prediction of the water displacement reaction energies demonstrate that the DFT M06L method gives closest results to those of MP2, than the widespread B3LYP functional.
5. The binding energy of DMSD is only a few kcal mol^{-1} inferior to that of HAM for Zn^{2+} and Fe^{2+} and is even slightly higher for the triplet state of $(NH_3)_3Ni^{2+}$ as revealed by MP2 and M06L methods.
6. All methods predict that both HAM and DMSD have stronger binding for the iron cation in the low spin state than for the high spin iron, although for nickel the inverse order of binding may be observed.
7. For both MBGs studied in the ammonia model the binding ability is nearly the same, i.e., $Fe^{2+}(t) > Ni^{2+}(t) > Fe^{2+}(q) > Ni^{2+}(s) > Zn^{2+}$. For the imidazole model the order is slightly different, i.e., $Ni^{2+}(t) > Fe^{2+}(t) > Fe^{2+}(q) > Ni^{2+}(s) \geq Zn^{2+}$.
8. Two types of intermediate complexes in the reaction of the water displacement from the $[(NH_3)_3M\text{-}OH_2]^{2+}$

model of metalloprotease, which differ by the direction of the attack of MBG, were found. Complexes formed by the back-side attack of HAM (in the direction opposite to a water molecule) on the models of zinc protease and high spin states of iron and nickel models are trigonal bipyramidal and have monodentate bonding to the MBG, while for those originating from the front-side attack the bidentate character of bonding increases and complexes have a structure of a distorted octahedron.

9. All intermediate complexes with the silanediol group, exception made of the back-side complex for zinc, are hexacoordinated with a bidentate bonding to the oxygen atoms of the silanediol group.
10. All intermediate complexes with imidazole ligands have octahedral structure with bidentate bonding of MBGs.
11. Complexation energies of these complexes are substantially lower that corresponding complexes with ammonia ligands but the tendencies are similar: energies are close for HAM and DMSD and they decrease on going from nickel to zinc.

References

1. Vallee BL, Auld DS (1993) Zinc: biological function and coordination motifs. Acc Chem Res 26:543–551
2. Maret W, Li Y (2009) Coordination dynamics of zinc in proteins. Chem Rev 109:4682–4707
3. Lipscomb WN, Sträter N (1996) Recent advances in zinc enzymology. Chem Rev 96:2375–2433
4. Holm RH, Kennepohl P, Solomon EI (1996) Structural and functional aspects of metal sites in biology. Chem Rev 96:2239–2314
5. Finnin MS, Donigian JR, Cohen A, Richon VM, Rifkind RA, Marks PA, Breslow R, Pavletich NP (1999) Structures of a histone deacetylase homologue bound to the TSA and SAHA inhibitors. Nature 401:188–193
6. Vannini A, Volpari C, Filocamo G, Casavola EC, Brunetti M, Renzoni D, Chakravarty P, Paolini C, De Francesco R, Gallinari P, Steinkuhler C, Di Marco S (2004) Crystal structure of a eukaryotic zinc-dependent histone deacetylase, human HDAC8, complexed with a hydroxamic acid inhibitor. Proc Natl Acad Sci USA 101:15064–15069
7. Somoza JR, Skene RJ, Katz BA, Mol C, Ho JD, Jennings AJ, Luong C, Arvai A, Buggy JJ, Chi E, Tang J, Sang BC, Verner E, Wynands R, Leahy EM, Dougan DR, Snell G, Navre M, Knuth MW, Swanson RV, McRee DE, Taric LW (2004) Structural snapshots of human HDAC8 provide insights into the class I histone deacetylases. Structure 12:1325–1334
8. Becker A, Schlichting I, Kabsch W, Groche D, Schultz S, Wagner AFV (1998) Iron center, substrate recognition, and mechanism of peptide deformylase. Nat Struct Biol 5:1053–1058
9. Madison V, Duca J, Bennett F, Bohanon S, Cooper A, Chu M, Desai J, Girijavallabhan V, Hare R, Hruza A, Hendrata S, Huang Y, Kravec C, Malcolm B, McCormick J, Miesel L, Ramamanathan L, Reichert P, Saksena A, Wang J, Weber PC, Zhu H, Fischmann T (2002) Binding affinities and geometries of various metal ligands in peptide deformylase inhibitors. Biophys Chem 101–102:239–247
10. Natesh R, Schwager SLU, Sturrock ED, Acharya KR (2003) Crystal structure of the human angiotensin-converting enzyme-lisinopril complex. Nature 421:551–554
11. Christianson DW, Lipscomb WN (1989) Carboxypeptidase A. Acc Chem Res 22:62–69
12. Mock WL, Zhang JZ (1991) Mechanistically significant diastereoselection in the sulfoximine inhibition of carboxypeptidase A. J Biol Chem 266:6393–6400
13. Fersht AR (1999) Enzyme structure and mechanism in protein science. Freeman, New York
14. Wu S, Zhang C, Xu D, Guo H (2010) Catalysis of carboxypeptidase A: promoted-water vs nucleophilic pathways. J Phys Chem B114:9259–9267
15. Gupta SP (2007) Quantitative structure-activity relationship studies on zinc-containing metalloproteinase inhibitors. Chem Rev 107:3042–3087
16. Farkas E, Katz Y, Bhusare S, Reich R, Röschenthaler G-V, Königsmann M, Breuer E (2004) Carbamoylphosphonate Based Matrix Metalloproteinase (MMP) inhibitor metal complexes - solution studies and stability constants. Towards a zinc selective binding group. J Biol Inorg Chem 9:307–315
17. Massie BM (1998) 15 years of heart-failure trials: what have we learned. Lancet 352(suppl I):SI29–33
18. Burnier M, Brunner HR (2000) Angiotensin II receptor antagonists. Lancet 355:637–45
19. Babine RE, Bender SL (1997) Molecular recognition of protein-minus signligand complexes: applications to drug design. Chem Rev 97:1359–1472
20. Vane JR (1999) The history of inhibitors of angiotensin converting enzyme. J Physiol Pharmacol 50:489–498
21. Borkakoti N (2004) Matrix metalloprotease inhibitors: design from structure. Biochem Soc Trans 32:17–22
22. Sieburth SM, Nittoli T, Mutahi AM, Guo L (1998) Silanediols-A new class of potent protease inhibitor. Angew Chem Int Ed 37:812–814
23. Chen CA, Sieburth SM, Glekas A, Hewitt GW, Trainor GL, Erickson-Viitanen S, Garber SS, Cordova B, Jeffry S, Klabe RM (2001) Drug design with a new transition state analog of the hydrated carbonyl: silicon-based inhibitors of the HIV protease. Chem Biol 8:1161–1166
24. Mutahi MW, Nittoli T, Guo L, Sieburth SM (2002) Silicon-based metalloprotease inhibitors: synthesis and evaluation of silanol and silanediol peptide analogues as inhibitors of angiotensin-converting enzyme. J Am Chem Soc 124:7363–7375
25. Kim J, Glekas A, Sieburth SM (2002) Silanediol-based inhibitor of thermolysin. Bioorg Med Chem Lett 12:3625
26. Juers DH, Kim J, Matthews BW, Sieburth SM (2005) Structural analysis of silanediols as transition-state-analogue inhibitors of the benchmark metalloprotease thermolysin. Biochem 44:16524–16528
27. El Yazal J, Pang YP (1999) Novel stable configurations and tautomers of the neutral and deprotonated hydroxamic acids predicted from high-level Ab initio calculations. J Phys Chem A 103:8346–8350
28. El Yazal J, Pang YP (1999) Ab initio calculations of proton dissociation energies of zinc ligands: hypothesis of imidazolate as zinc ligand in proteins. J Phys Chem B 103:8773–8779
29. El Yazal J, Pang YP (2000) Proton dissociation energies of zinc-coordinated hydroxamic acids and their relative affinities for zinc: insight into design of inhibitors of zinc- containing proteinases. J Phys Chem B 104:6499–6504
30. Deerfield DW, Carter C, Pedersen LG (2001) Models for protein–zinc ion binding sites II. The catalytic sites. Int J Quant Chem 83:150–165

31. Remko M, Garaj V (2003) Thermodynamics of binding of Zn2+ to carbonic anhydrase inhibitors. Mol Phys 101:2357–2368
32. Cheng F, Zhang R, Luo X, Shen J, Li X, Gu J, Zhu W, Shen J, Sagi I, Ji R, Chen K, Jiang H (2002) Quantum chemistry study on the interaction of the exogenous ligands and the catalytic zinc ion in matrix metalloproteinases. J Phys Chem B 106:4552–4559
33. Khandelwal A, Lukacova V, Comez D, Kroll DM, Raha S, Balaz S (2005) A combination of docking, QM/MM, and MD simulation for binding affinity estimation of metalloprotein ligands. J Med Chem 48:5437–5447
34. Linder DP, Rodgers KR (2004) Theoretical study of imidazole- and thiol-based zinc binding groups relevant to inhibition of metzincins. J Phys Chem B 108:13839–13849
35. Šramko M, Garaj V, Remko M (2008) Thermodynamics of binding of angiotensin-converting enzyme inhibitors to enzyme active site model. J Mol Struct (THEOCHEM) 869:19–28
36. Dobbs KD, Rinehart AM, Howard MH, Zheng YJ, Kleier DA (2006) Computational characterization of metal binding groups for metalloenzyme inhibitors. J Chem Theor Comput 2:990–996
37. Vanommeslaeghe K, Loverix S, Geerlings P, Tourwé D (2005) DFT-based ranking of zinc-binding groups in histone deacetylase inhibitors. Bioorg Med Chem 13:6070–6082
38. Vanommeslaeghe K, Van Alsenoy C, De Proft F, Martins JC, Tourwé D, Geerlings P (2003) Ab initio study of the binding of Trichostatin A (TSA) in the active site of histone deacetylase like protein (HDLP). Org Biomol Chem 1:2951–2957
39. Vanommeslaeghe K, De Proft F, Loverix S, Tourwé D, Geerlings P (2005) Theoretical study revealing the functioning of a novel combination of catalytic motifs in histone deacetylase. Bioorg Med Chem 13:3987–3992
40. Corminboef C, Hu P, Tuckerman ME, Zhang Y (2006) Unexpected deacetylation mechanism suggested by a density functional theory QM/MM study of histone-deacetylase-like protein. J Am Chem Soc 128:4530–4531
41. Frison G, Ohanessian G (2008) A comparative study of semiempirical, ab initio, and DFT methods in evaluating metal-ligand bond strength, proton affinity, and interactions between first and second shell ligands in Zn-biomimetic complexes. J Comput Chem 29:416–433
42. Elstner M, Cui Q, Munih P, Kaxiras E, Frauenheim T, Karplus M (2003) Modeling Zinc in biomolecules with the self consistent charge-density functional tight binding (SCC-DFTB) method: Applications to structural and energetic analysis. J Comput Chem 24:565–581
43. Marmion CJ, Griffith D, Nolan KB (2004) Hydroxamic acids - an intriguing family of bioligands and enzyme inhibitors. Eur J Inorg Chem 15:3003–3016
44. Codd R (2008) Traversing the coordination chemistry and chemical biology of hydroxamic acids. Coord Chem Rev 252:1387–1408
45. Wang D, Helquist P, Wiest O (2007) Zinc binding in HDAC inhibitors: a DFT study. J Org Chem 72:5446–5449
46. Wu R, Lu Z, Cao Z, Zhang Y (2011) Zinc chelation with hydroxamate in histone deacetylases modulated by water access to the linker binding channel. J Am Chem Soc 133:6110–6113
47. Becke AD (1993) Density-functional thermochemistry III. The role of exact exchange. J Chem Phys 98:5648–5652
48. Lee C, Yang W, Parr RG (1988) Development of the Colle-Salvetti conelation energy formula into a functional of the electron density. Phys Rev B 37:785–789
49. Zhao Y, Truhlar DG (2006) A new local density functional for main-group thermochemistry, transition metal bonding, thermochemical kinetics, and noncovalent interactions. J Chem Phys 125:194101
50. Zhao Y, Truhlar DG (2008) The M06 suite of density functionals for main group thermochemistry, thermochemical kinetics, noncovalent interactions, excited states, and transition elements: two new functionals and systematic testing of four M06-class functionals and 12 other functionals. Theor Chem Acc 120:215–241
51. Amin EA, Truhlar DG (2008) Zn coordination chemistry: development of benchmark suites for geometries, dipole moments, and bond dissociation energies and their use to test and validate density functionals and molecular orbital theory. J Chem Theor Comput 4:75–85
52. Sorkin A, Iron MA, Truhlar DG (2008) Density functional theory in transition-metal chemistry: relative energies of low-lying states of iron compounds and the effect of spatial symmetry breaking. J Chem Theor Comput 4:307–315
53. Cramer CJ, Truhlar DG (2009) Density functional theory for transition metals and transition metal chemistry. Phys Chem Chem Phys 11:10757–10816
54. Zeng Y, Wang S, Feng H, Xie Y, King RB (2011) Highly unsaturated binuclear butadiene iron carbonyls: quintet spin States, perpendicular structures, agostic hydrogen atoms, and iron-iron multiple bonds. Int J Mol Sci 12:2216–2231
55. Binkley JS, Pople JA (1975) Møller–Plesset theory for atomic ground state energies. Int J Quant Chem 9:229–236
56. Grimme S, Antony J, Ehrlich S, Krieg H (2010) A consistent and accurate ab initio parametrization of density functional dispersion correction (DFT-D) for the 94 elements H-Pu. J Chem Phys 132:154104
57. Woon DE, Dunning TH (1993) Gaussian basis sets for use in correlated molecular calculations. III. The atoms aluminum through argon. J Chem Phys 98:1358–1371
58. Frisch MJ et al. (2009) Gaussian 09, Revision B.01. Gaussian, Wallingford
59. Reed AE, Curtiss LA, Weinhold F (1988) Intermolecular interactions from a natural bond orbital, donor-acceptor viewpoint. Chem Rev 88:899–926
60. Glendening ED, Reed AE, Carpenter JE, Weinhold F (1988) NBO v3.1, Madison
61. Akesson R, Pettersson LGM, Sandstrom M, Siegbahn PEM, Wahlgrent U (1993) Theoretical study of water-exchange reactions for the divalent ions of the first transition period. J Phys Chem 97:3765–3774
62. Dudev T, Lim C (2003) Principles governing Mg, Ca, and Zn binding and selectivity in proteins. Chem Rev 103:773–788
63. He H, Puerta DT, Cohen SM, Rodgers KR (2005) Spectroscopic study of reactions between chelating zinc-binding groups and mimics of the MMP and ADAM catalytic sites: the coordination chemistry of metalloprotease inhibition. Inorg Chem 44:7431–7442
64. Bertrand P (2010) Inside HDAC with HDAC inhibitors. Eur J Med Chem 45:2095–2116